Exp Fluids (2009) 46:109–119
DOI 10.1007/s00348-008-0544-y

RESEARCH ARTICLE

On the spatial resolution of velocity and velocity gradient-based turbulence statistics measured with multi-sensor hot-wire probes

**P. V. Vukoslavčević · N. Beratlis · E. Balaras ·
J. M. Wallace · O. Sun**

Received: 1 February 2008 / Revised: 16 June 2008 / Accepted: 7 July 2008 / Published online: 7 August 2008
© Springer-Verlag 2008

Abstract A highly resolved turbulent channel flow direct numerical simulation with $Re_\tau = 200$ has been used to investigate the ability of 12-sensor hot-wire probes to accurately measure velocity and velocity gradient based turbulence statistics. Various virtual sensor separations have been tested in order to study the effects of spatial resolution on the measurements. First, the effective cooling velocity has been determined for each sensor for (1) an idealized probe where the influence of the velocity component tangential to the sensors and flow blockage by the presence of the prongs and the finite lengths of and thermal cross-talk between the sensors are neglected and, (2) for a real probe, the characteristics of which have been determined experimentally. Then, simulating the response of the virtual probes for these two cases to obtain the effective velocities cooling the sensors, velocity and vorticity component statistics have been calculated by assuming the velocity gradients to be constant over the probe sensing area.

1 Introduction

The use of numerical simulations to investigate the response characteristics of hot-wire probes to turbulent flow fields has provided new insight into sources of measurement error for this frequently used experimental technique. Of particular importance has been the insight gained regarding the effects of the spatial separation between sensors of multi-sensor probes on measured flow properties. These effects occur because all hot-wire probes are exposed to a spatially varying instantaneous velocity field when the flow is turbulent, but this fact is necessarily neglected in the response equations for all but the most complex probes. Even when such complex probes take this velocity field variation into account, they rarely have been able to account for its non-linear variation.

Using a turbulent boundary layer direct numerical simulation (DNS) database, Moin and Spalart (1987) studied the spatial resolution effects on the response of an X-array probe with sensor separations of one viscous length as well as the effects of the velocity components in the direction of the sensors' separation. The probe's sensors were modeled as two points in the simulated flow, thus the finite sensor lengths were not accounted for. Even with this small sensor separation, they found that the wall normal velocity component root-mean-square (rms) values were significantly overestimated near the wall. Suzuki and Kasagi (1992) extended this type of probe response analysis by varying the sensor separation of X- and V-array probes in various orientations in a turbulent channel flow DNS. They found

---

P. V. Vukoslavčević
Masinski Fakultet, University of Montenegro,
81000 Podgorica, Montenegro
e-mail: petarvu@ac.me

N. Beratlis · E. Balaras (✉) · J. M. Wallace
Department of Mechanical Engineering, University of Maryland,
College Park, MD 20742, USA
e-mail: balaras@umd.edu

N. Beratlis
e-mail: nikosb@umd.edu

J. M. Wallace
e-mail: wallace@umd.edu

O. Sun
Department of Mechanical Engineering,
Johns Hopkins University, Baltimore,
MD 21218, USA
e-mail: osun@jhu.edu

that, although the effects of the out-of-supporting-prongs-plane velocity components are quite small, the rms values of the cross-stream components were greatly overestimated near the wall with increasing sensor separation while the streamwise component rms values were only slightly underestimated. They proposed a correction method which depends on the knowledge of two-point correlation coefficients in the flow region where the measurements are to take place—something, however, usually not available to experimenters. Tagawa et al. (1992) drew similar conclusions about the large errors in the wall-normal velocity component caused by sensor separation by using a simulated Gaussian velocity field to reproduce typical wall turbulence conditions. Pompeo and Thomann (1993) compared the values of various turbulence statistics from a turbulent channel flow DNS to those from a four-sensor probe with various sensor arrangements. All the sensors were modeled as points in the simulated flow, and the results were compared to laboratory measurements of a real four-sensor probe. Consistent with previous studies, they also found that the errors became quite large with increasing sensor separations.

Park and Wallace (1993) independently confirmed the conclusions of Suzuki and Kasagi (1992) and others by synthetically studying the response of two- and four-sensor probes to an experimental nine-sensor probe turbulent boundary layer database that provided velocity gradient tensor as well as the velocity vector component information. For the largest sensor separation they investigated, $S^+ = 9$ (where + indicates normalization with the friction velocity, u_τ, and kinematic viscosity, ν), the four-sensor configuration resulted in a 43% greater wall-normal velocity rms, a 19% greater spanwise velocity rms and a 33% greater streamwise vorticity rms than the nine-sensor probe database values for $y^+ = 30$ at the upper edge of the buffer layer. Petrović et al. (2003) carried out a similar investigation using a 12-sensor probe boundary layer data base. Having studied combinations of two-, three-, four- and nine-sensors, they concluded that the wall-normal and spanwise instantaneous velocity gradients have the largest influence on the errors. Wyngaard (1969) theoretically examined the spatial resolution effects on measurements of streamwise vorticity for isotropic turbulence with a four-sensor probe configured like that of Park and Wallace (1993). He recommended that the ratio of sensor lengths to the Kolmogorov scale should not be smaller than 3.3 to avoid significant attenuation of the measured variance.

This paper examines the dependence on spatial resolution of important velocity and velocity gradient-based statistical properties of turbulence measured with multi-sensor hot-wire probes. For example, to determine the vorticity vector and the strain rate tensor it is necessary to simultaneously measure all the elements of the instantaneous velocity gradient tensor. To do this with hot-wire anemometry at least three arrays of three sensors each, separated in the cross-stream, y and z, directions, are needed (Wallace and Foss 1995). To provide some redundancy and more accuracy, usually three arrays of four sensors are used for a total of 12 sensors. Determination of the three streamwise gradients is possible using Taylor's hypothesis (Taylor 1938) or even by placing some of the sensors upstream of the others as in Galanti et al. (2004). With eight sensors it is also possible to estimate all three components of the vorticity vector when Taylor's hypothesis is utilized. Several investigators have made such measurements with eight- and nine-sensor probes in turbulent boundary layers (Balint 1986; Vukoslavčević et al. 1991; Balint et al. 1991; Wallace et al. 1992; Ong and Wallace 1995; Ong and Wallace 1998; Andreopoulos and Honkan 1996; Honkan and Andreopoulos 1997; Andreopoulos and Honkan 2001) and grid flows (Kit et al. 1988; Wallace et al. 1992; Antonia et al. 2002). Others have used 12-sensor probes in boundary layers (Tsinober et al. 1992; Vukoslavčević and Wallace 1996; Folz 1997), wakes (Marasli et al. 1993), mixing layers (Loucks 1998), jets (Cavo et al. 2007) and grid flows (Tsinober et al. 1992). Twenty and 21-sensor probes have even been used for such measurements in boundary layers (Lemonis 1995), grid flows (Lemonis 1995) and the atmospheric surface layer (Kholmyansky et al. 2001; Galanti et al. 2004). Details about the configurations of such probes, their fabrication and many of their performance characteristics are given in Vukoslavčević and Wallace (2007).

Zhu and Antonia (1996) studied analytically the effects of the spatial resolution of their eight-sensor probe, and devised a method to correct the vorticity component variances and their spectra. To date, however, little is known about the effects of spatial resolution on the accuracy of important statistical properties of turbulence measured with other multi-sensor probes with nine or more sensors, particularly on those properties derived from the velocity gradient tensor, such as strain-rate, dissipation rate, and vorticity. To further examine the spatial resolution question we have used a highly resolved turbulent channel flow DNS to simulate the responses of a 12-sensor probe for various sensor separations.

2 The 12-sensor probe

A 12-sensor probe, capable of simultaneous measurements of all three velocity components and the velocity gradients in the $y{-}z$ plane is shown in the photograph and sketch in Fig. 1. The characteristic probe dimensions are the array separations, S_y and S_z and the prongs separation, b. One of the most widely used expressions describing the effective

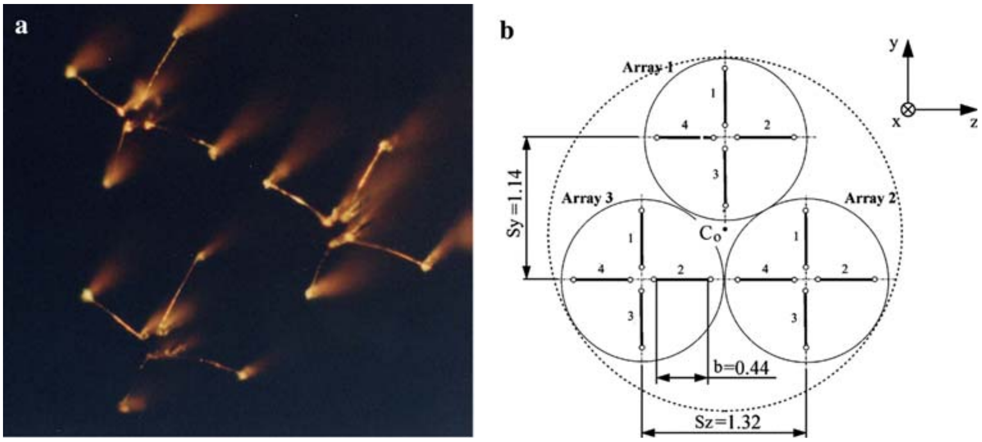

Fig. 1 Photograph of 12-sensor probe and front view sketch. Typical dimensions in mm

velocity, U_e, cooling each hot-wire sensor in a three dimensional turbulent flow field is that proposed by Jorgensen (1971),

$$U_e^2 = U_n^2 + k^2 U_t^2 + h^2 U_b^2, \tag{1}$$

where U_n, U_t and U_b are the orthogonal components of the velocity vector with respect to the sensor coordinate system, i.e. normal, tangential and binormal to the sensor, while k and h are the so-called yaw and pitch coefficients that take into account flow distortion by the prongs and thermal and finite sensor length effects. Replacing the orthogonal velocity components U_n, U_t and U_b in Jorgensen's expression with U, V and W, the streamwise, cross-stream and spanwise velocity components in the flow coordinate system, the following expressions for the response of the jth ($j = 1-4$) sensor of the ith ($i = 1-3$) array is obtained:

$$U_{e_{ij}}^2 = a_{ij1} U_{ij}^2 + a_{ij2} V_{ij}^2 + a_{ij3} W_{ij}^2 + a_{ij4} U_{ij} V_{ij} + a_{ij5} U_{ij} W_{ij} + a_{ij6} V_{ij} W_{ij}. \tag{2}$$

The coefficients a_{ijk} ($k = 1-6$) are products of sines and cosines of the sensor angle orientations α and of the pitch and yaw coefficients, h and k, of each sensor. For an ideal probe with specified sensor angle orientations and without prong interference and thermal and finite sensor length effects, i.e. $k = 0$ and $h = 1$, they can be defined analytically as shown in the Appendix. For a real probe an adequate calibration procedure is required to determine the a_{ijk}. The velocity components U_{ij}, V_{ij} and W_{ij} can be defined in terms of the velocity components U_0, V_0 and W_0 at the probe center, C_0 (see Fig. 1), their gradients in the cross-stream plane, i.e. the plane normal to the probe axis that passes through the sensor centers, and the distances c_{ij} and d_{ij} in the y and z directions between C_0 and the centers of each sensor.

Expanding the velocity components U_0, V_0 and W_0 to first order in a Taylor series about C_0 results in the following 12 nonlinear algebraic approximate equations with nine velocity component and cross-stream velocity gradient unknowns:

$$\begin{aligned} U_{e_{ij}}^2 \approx\ & a_{ij1}(U_0 + gU_{ij})^2 + a_{ij2}(V_0 + gV_{ij})^2 \\ & + a_{ij3}(W_0 + gW_{ij})^2 + a_{ij4}(U_0 + gU_{ij}) \\ & \times (V_0 + gV_{ij}) + a_{ij5}(U_0 + gU_{ij})(W_0 + gW_{ij}) \\ & + a_{ij6}(V_0 + gV_{ij})(W_0 + gW_{ij}), \end{aligned} \tag{3}$$

where

$$gU_{ij} = c_{ij}\frac{\partial U}{\partial y} + d_{ij}\frac{\partial U}{\partial z} \tag{4}$$

and with U replaced by V and W for gV_{ij} and gW_{ij}. The c_{ij} and d_{ij} constants can be expressed as positive or negative fractions of the prong spacings b projected on this cross-stream plane for a given probe geometry.

In these response equations, the velocity gradients in the cross-stream plane experienced by the sensors, $\partial U_i/\partial x_j$, with ($U_i = U$, V, W) and ($j = y$, z), are assumed to be constant over the probe measurement region, i.e. the velocity field is assumed to vary linearly over the sensors and probe. The accuracy of this approximation obviously depends on the lengths of the sensors and the distances between the array centers, i.e. on the spatial resolution of the probe.

3 Physical experiment

In a real physical experiment the effective velocity cooling each sensor $U_{e_{ij}}$ can be found from King's law

$$E_{ij}^2 = A + BU_{e_{ij}}^n, \tag{5}$$

where E is the anemometer voltage responding to U_e, and A, B and n are parameters determined by calibration. U_e can also be found from a polynomial fit of the data of the form

$$\sum_{p=1}^{5} b_p E_{ij}^{p-1} = U_{e_{ij}}^2, \tag{6}$$

where the b_p are coefficients of the polynomial in E_{ij}. In this investigation (6) was used. None of the coefficients in the above equations need to be known in advance. They can be determined with a calibration procedure. Only the distances between the probe center, C_0 and the array centers, c_{ij} and d_{ij}, have to be measured, and they must be determined very accurately. How the a_{ijk} and b_p coefficients are obtained by calibration is described in the Appendix.

A numerical algorithm is used to solve the system of equations in (3) iteratively to obtain the three velocity components at the probe center and the six velocity gradients in the y and z directions. A special feature of this algorithm is that, for each array, it chooses the three sensor response equations, out of the four available, that give the maximum uniqueness range for the solution (see Vukoslavčević and Wallace 1996 for details).

4 Virtual experiment

To simulate the response of a 12-sensor probe and to investigate its spatial resolution, the sensors can be simply modeled as points arranged in the appropriate probe geometry and located on the mesh of a DNS. The relative positions of these points can thus be varied to study spatial resolution effects. A more complex analysis in which the variation of the velocity field along finite length sensors could be undertaken, but the simplified approach taken here is an appropriate prior step. To obtain a highly resolved DNS, a minimal turbulent channel flow (Jimenez and Moin 1998) was simulated for a Reynolds number $Re_\tau = 200$, where $Re_\tau = u_\tau h/\nu$, and h is the channel half width. The equations of motion were solved using a fractional step method where both advective and diffusive terms were treated explicitly using an Adams–Bashforth scheme. All spatial derivatives were discretized with second-order, central finite differences on a staggered grid. The details of the numerical methodology together with applications in wall-bounded and free-shear flows can be found in Piomelli et al. (2000) and Balaras et al. (2001). The size of the computational domain was set to $2h \times 2h \times h$ and was discretized using $400 \times 400 \times 200$ grid nodes in the streamwise, wall normal and spanwise directions, respectively. The grid was uniform in all directions, and the resulting resolution is $\Delta x^+ = \Delta y^+ = \Delta z^+ \approx 1$. This configuration permits the existence of about two low and high speed streaks as can be seen in Fig. 2. The variation of the Kolmogorov scale across the channel for this fixed grid spacing is also shown in Fig. 2. Near the wall the grid size Δ is about 1.5 times smaller in each coordinate direction than the Kolmogorov length η; near the channel centerline the resolution improves to approximately four times smaller. To be able to perform the virtual probe experiments a database of approximately 50 statistically independent instantaneous realizations over 15 eddy turnover times was generated. The sample was found to be sufficient to obtain converged statistics. The mean velocity and the root-mean-square (rms) velocity and vorticity fluctuations compared very well to those of Kim et al. (1987) at the same Reynolds number. Near the wall in the buffer layer at $y^+ = 15$ where the effects of spatial resolution are greatest, the ratios of the values of the spanwise microscales to the Kolmogorov scale η, to the maximum distance between supporting prongs b and to the spanwise maximum spacing between arrays examined here, as estimated from the DNS, are respectively: $\lambda_i/\eta = 12.3$, 8.4 and 16.8; $\lambda_i/b = 3.6$, 2.1 and 4.2 and $\lambda_i/S_z = 1.8$, 1.1 and 2.1, with $i = x,y$ and z. Thus, for the worse resolution examined here with $S_y^+ = S_z^+ = 12$, the spanwise microscale is over twice the spacing between arrays. For a physical experiments with $R_\tau \approx 1000$, like those in the references cited where such probes have been used, the ratios λ_i/S_z will be smaller than for the DNS at $R_\tau = 200$ considered here. In such cases, typically S_y and S_z would be about $\frac{2}{3}\lambda$. A virtual probe is shown in Fig. 3 with array separations S_y and S_z of eight mesh cells Δy and Δz. This separation between arrays was varied between 2 and 12, and the separation between

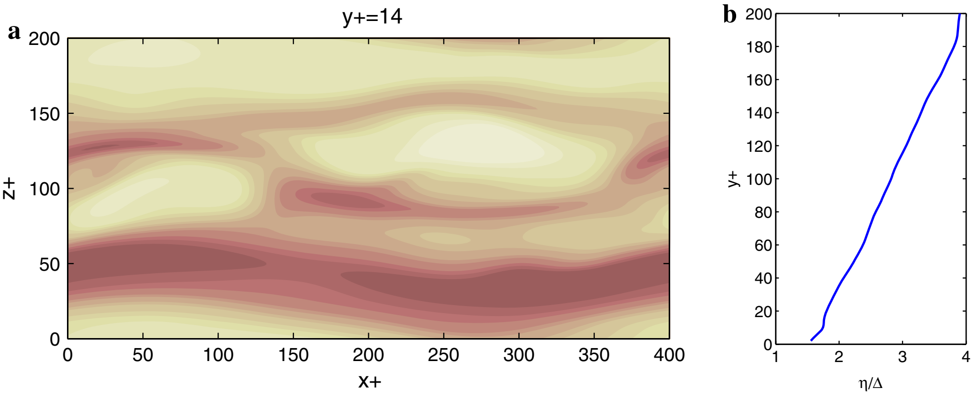

Fig. 2 **a** Contours of the streamwise velocity fluctuations in the minimal turbulent channel flow showing low- and high-speed streaks; **b** comparison of grid size Δ to Kolmogorov length η across the channel

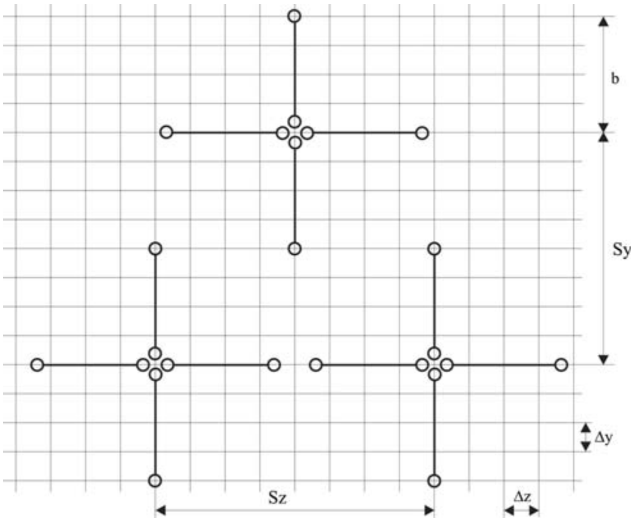

Fig. 3 Sketch of 12-sensor probe represented as points on a DNS mesh with $\Delta x^+ = \Delta y^+ = \Delta z^+ \approx 1$ resolution. Here the array separations are $S_y^+ = S_z^+ \approx 8$.

the virtual supporting prong locations was varied proportionately so that $S_y/b = S_z/b = 2$. Thus the size of each array was varied in this proportion with the distance between arrays. Other ratios could, of course, be studied, but this one is of greatest practical interest because it is the ratio corresponding to the minimum array separations for a given value of b. When the sensor centers coincide with the nodes of the grid, the velocity components at each sensor center are equal to the velocity components at the corresponding node. Otherwise the velocity components at the sensor centers can be found by an adequate interpolation.

Using these simulated velocity components at the sensor centers, U_{ij}, V_{ij} and W_{ij}, the effective cooling velocity at each sensor center, U_{eij}, can be found from (2). The values of the probe coefficients, a_{ijk}, with $k = 1-6$ that are needed can be obtained theoretically for an ideal probe with $k = 0$ and $h = 1$, or the calibration coefficients of an actual probe can be used (see the Appendix). With these sets of coefficients and effective cooling velocities, three velocity components and six velocity gradients at the probe center can be obtained from (3) by applying the same numerical algorithm as in the case of the physical experiment. To obtain the streamwise velocity gradient values for all the resolution cases, we applied central differencing over three nodes from the DNS database. Because the DNS database was not temporally resolved, Taylor's hypothesis could not be incorporated in this investigation to obtain the values of the streamwse velocity gradients as would be done with a physical 12-sensor probe. This is, in fact, a virtue for this investigation because the spatial resolution effects are separated from those due to the use of Taylor's hypothesis.

By comparing the statistical properties of the simulated flow "measured" in this way by the virtual probe, with the same properties determined directly from the DNS, the influence of the probe's spatial resolution can be systematically examined. This is done for velocity statistics in Sect. 5, for the vorticity statistics in Sect. 6 and for the turbulent kinetic energy production and dissipation rates in Sect. 7.

5 Velocity

5.1 Root-mean-square velocity distributions and spectra

In Fig. 4 the rms distributions of the three velocity components, denoted by u', v' and w', are shown for the ideal probe cases. The distribution values with different resolutions are compared to the values of the DNS from which they are determined. For $S^+ = 2$ and 4, there is very little attenuation of the fluctuation rms values throughout the channel half width (only $y^+ \leq 100$ is plotted in this and subsequent figures to emphasize the wall region where the resolution effects are evident). For $S^+ = 8$, which is a slightly better resolution than that of probes used in several of the experiments cited in the Introduction (Vukoslavčević et al. 1991; Balint et al. 1991; Wallace et al. 1992; Ong and Wallace 1995; Ong and Wallace 1998; Loucks 1998), the peak of u' is attenuated by about 7% at $y^+ \approx 15$. The v' distribution varies differently near the wall from the other cases with $S^+ = 12$. This shape appears to be a real resolution effect, because it is also evident for $S^+ = 10$ which is not plotted in the figure.

Also shown in Fig. 4 are the rms values for $S^+ = 8$ calculated with the experimental probe coefficients. The values are almost identical to those for the ideal probe with the same resolution, which is a clear indication that the experimental probe calibration coefficients account very well for flow blockage and thermal cross-talk between sensors and their finite length, effects which are not considered with the ideal coefficients.

The k_x spectra for the streamwise velocity component at $y^+ = 18$ are shown Fig. 5. Consistent with the rms distribution attenuation effects, at higher values of the wavenumber the spectra roll off at a steeper rate with increasing sensor array separation, up until the $k_x\eta$ values where the unresolved energy begins to pile up and the spectra turn upward.

5.2 Velocity fluctuation skewness and flatness factor distributions

The skewness factors for the velocity fluctuations are shown in Fig. 6. The skewness factor values for the spanwise velocity fluctuations, S_w, oscillate slightly around

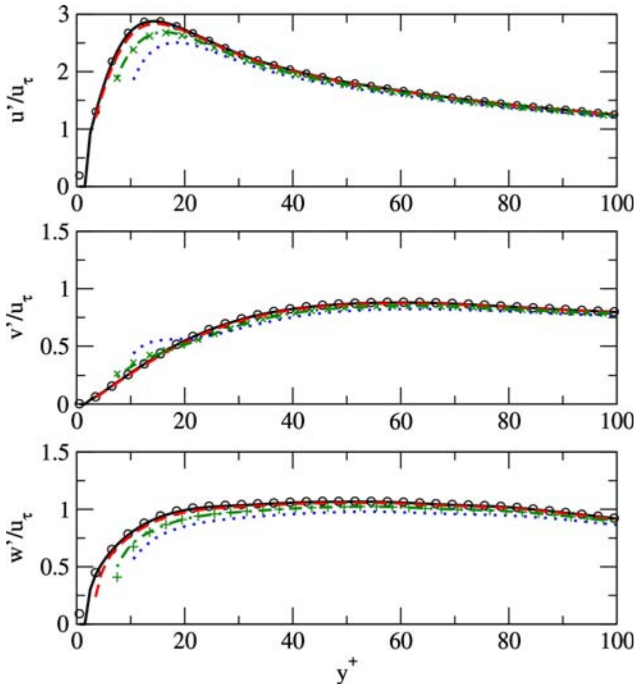

Fig. 4 Attenuation of the velocity component rms values with increasing sensor array separations. *Small circle* DNS data; *solid line* $S^+ = 2$; *dashed line* $S^+ = 4$; *dash with dotted line* $S^+ = 8$; *dotted line* $S^+ = 12$ (determined with ideal coefficients); *cross* $S^+ = 8$ (determined with experimental coefficients)

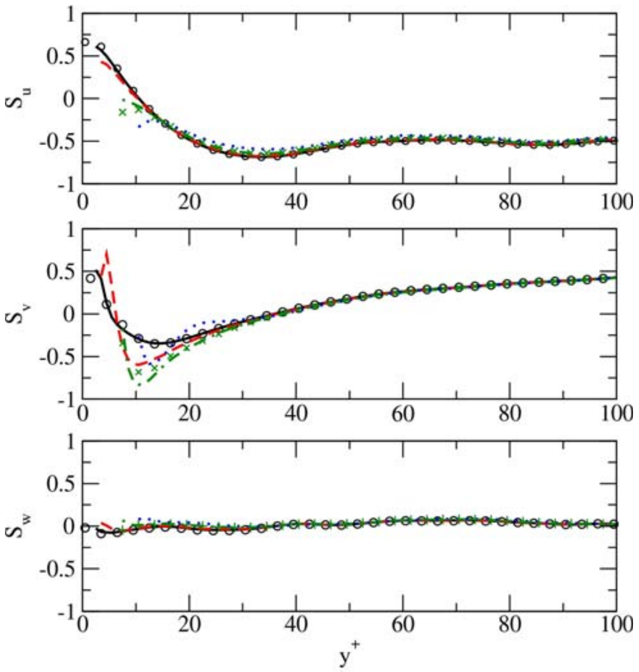

Fig. 6 Resolution effects on the velocity component skewness factor values with increasing sensor array separations. *Small circle* DNS data; *solid line* $S^+ = 2$; *dashed line* $S^+ = 4$; *dashed with dotted line* $S^+ = 8$; *dotted line* $S^+ = 12$ (determined with ideal coefficients); *cross* $S^+ = 8$ (determined with experimental coefficients)

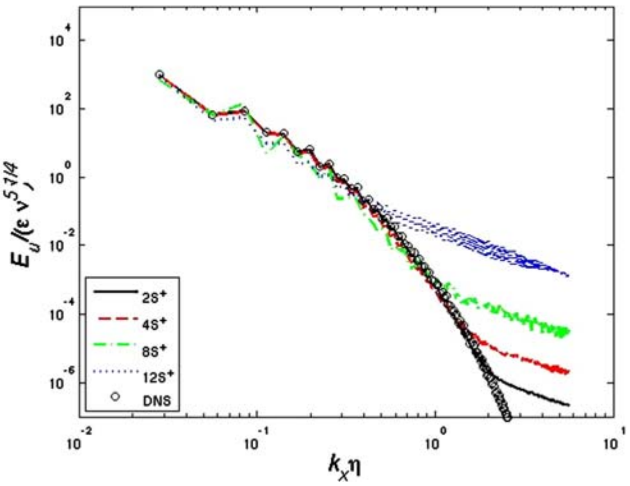

Fig. 5 Streamwise velocity fluctuation k_x spectra at $y^+ = 18$ with increasing sensor array separations compared to the DNS spectra. Normalization with Kolmogorov scaling

zero, as they should because of the symmetry of the mean flow. That the DNS and high resolution ($S^+ = 2$ and 4) values are not precisely zero is probably due to a combination of the minimal channel effects and, perhaps, a somewhat too small data sample size. However, the maximum deviation from zero is less than 0.1. The greatest resolution effects are seen for the skewness of the wall normal component, S_v. The peak negative values, which lie between $y^+ = 12-15$, become much more negative than the DNS values with increasing sensor array separation until the shape of the distribution changes for $S^+ = 12$ when the negative peak diminishes. As for the rms, this is a real resolution effect because it is also seen for $S^+ = 10$, which is not plotted. Values of the skewness of the v velocity fluctuations found in the literature exhibit a great deal of scatter in the buffer layer for turbulent channel flows and boundary layers. The present investigation indicates that this is likely due to the wide range of spatial resolutions of the probes that were used in those experiments and in those simulations.

The values for the $S^+ = 8$ case with experimental probe coefficients are also shown in the figure. At its most negative, the skewness values for the $S^+ = 8$ case with experimental coefficients are only a little less negative than with the ideal probe coefficients.

There is very little effect of probe resolution on the flatness factor values of the streamwise velocity fluctuations, F_u, as seen in Fig. 7, although the shape of the $S^+ = 12$ distribution is altered a bit. Near the wall the effects for the lower resolution cases, $S^+ = 8$ and 12, on F_v and F_w are quite large. Except for the locations closest to the wall, the $S^+ = 8$ cases with ideal and experimental coefficients agree very well with each other.

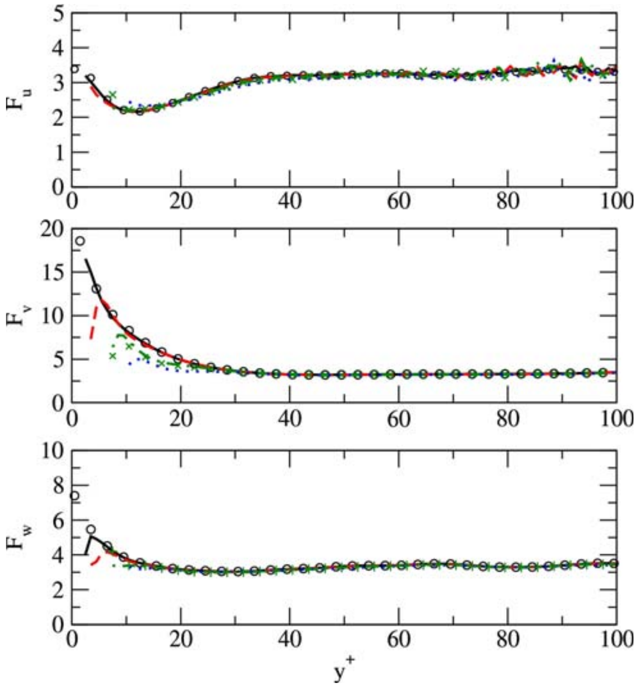

Fig. 7 Resolution effects on the velocity component flatness factor values with increasing sensor array separations. *Small circle* DNS data; *solid line* $S^+ = 2$; *dashed line* $S^+ = 4$; *dashed with dotted line* $S^+ = 8$; *dotted line* $S^+ = 12$ (determined with ideal coefficients); *cross* $S^+ = 8$ (determined with experimental coefficients)

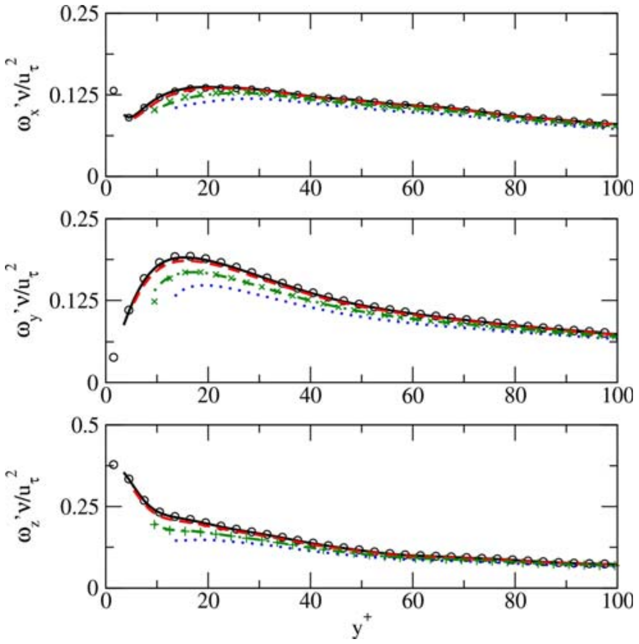

Fig. 8 Attenuation of the vorticity component rms values with increasing sensor array separations. *Small circle* DNS data; *solid line* $S^+ = 2$; *dashed line* $S^+ = 4$; *dash with dotted line* $S^+ = 8$; *dotted line* $S^+ = 12$ (determined with ideal coefficients); *cross* $S^+ = 8$ (determined with experimental coefficients). Normalization with viscous time scale, ν/u_τ^2

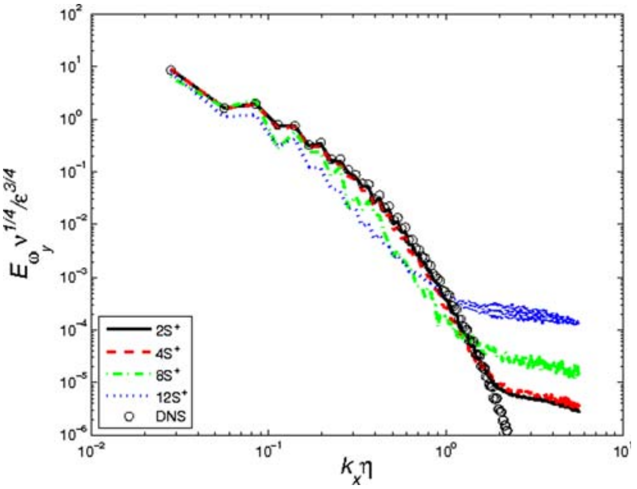

Fig. 9 Wall normal vorticity fluctuation k_x spectra at $y^+ = 15$ with increasing sensor array separations compared to the DNS spectra. Normalization with Kolmogorov scaling

6 Vorticity

6.1 Root-mean-square vorticity distributions and spectra

In Fig. 8 the greatest resolution effects are for the wall normal vorticity rms values, ω_y'. As for the velocity fluctuation rms values, almost no resolution effects are evident for the $S^+ = 2$ and 4 cases. For $S^+ = 8$, ω_y' is attenuated about 17% at $y^+ \approx 15$, and the simulation with experimental probe coefficients is identical to that with the ideal probe coefficients for this array separation. The attenuation with the $S^+ = 12$ separation is considerably larger, reaching about 27% at $y^+ \approx 15$.

The wall normal component k_x spectrum at $y^+ = 18$ is shown in Fig. 9. As for the streamwise velocity component spectrum, up until the unresolved energy pileup at high wavenumber, these vorticity component spectra roll off at a steeper rate with increasing sensor array separation, leading to lower peak rms values.

6.2 Vorticity fluctuation skewness and flatness factor distributions

The skewness factor values in Fig. 10 are within a range of ±0.25 of zero for both the streamwise and wall normal components, S_{ω_x} and S_{ω_y}. As for the velocity field, this deviation from the zero values, required by the mean flow symmetry conditions, are likely due to a combination of the minimal channel effects and, perhaps, a somewhat too small data sample size. The resolution effects on the spanwise vorticity skewness factor values occur all across the channel half width. With increasingly poorer

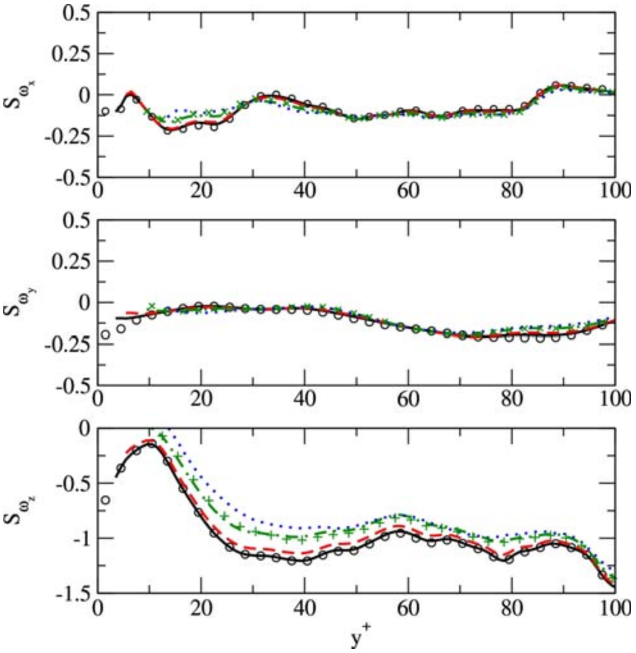

Fig. 10 Resolution effects on the vorticity component skewness factor values with increasing sensor array separations; *solid line* $S^+ = 2$; *dashed line* $S^+ = 4$; *dashed with dotted line* $S^+ = 8$; *dotted line* $S^+ = 12$ (determined with ideal coefficients); *cross* $S^+ = 8$ (determined with experimental coefficients)

resolution, the negative skewness factor diminishes in magnitude. For $S^+ = 8$ the results with ideal and experimental probe coefficients are practically identical.

The vorticity component flatness factor distributions for the three vorticity fluctuation components, seen in Fig. 11, are all affected by the probe resolution for all array separations and throughout the half width of the channel. The effects are particularly great for the wall normal component, ω_y. As for the other statistical properties, the simulated values with $S^+ = 8$ with the ideal and experimental coefficients track each other very closely.

7 Turbulent kinetic energy production and dissipation rate distributions

The production rate for turbulent kinetic energy in the transport equation for a fully developed channel flow is given by $\mathcal{P} = -\overline{uv}\partial\overline{U}/\partial x$. The mean velocity distribution is only slightly affected by the spatial resolution of the virtual probe. Therefore, almost all the resolution effects on the production rate are due to how the Reynolds shear stress, $-\overline{uv}$, is affected by the spatial resolution. The full dissipation rate expression is $\varepsilon = -\nu(\overline{(\partial u_i/\partial x_j)}^2 + \overline{\partial u_i/\partial x_j\, \partial u_j/\partial x_i})$. To estimate the effect of spatial resolution of the virtual probe on the dissipation rate, the cross-stream gradients obtained with the different spatial resolutions were used in this expression. As describe in Sect. 4, the streamwise gradients obtained by central differencing over three points from the DNS were used in this calculation for all the virtual probe resolutions.

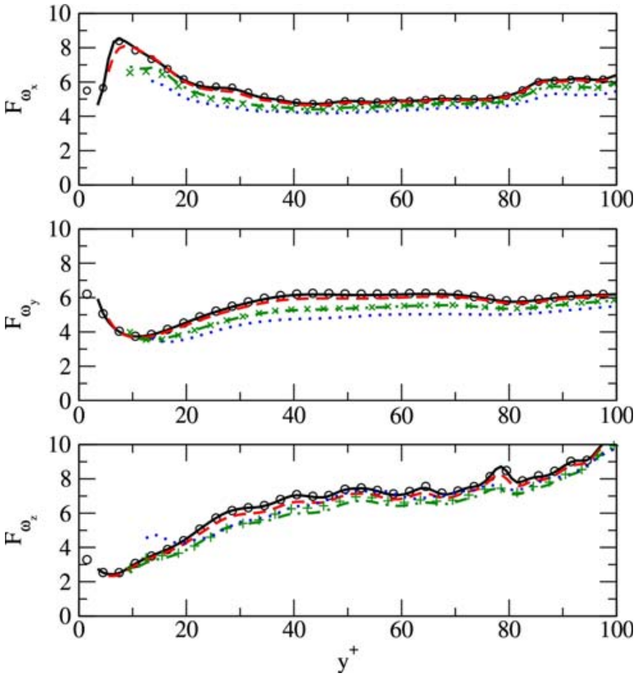

Fig. 11 Resolution effects on the vorticity component skewness factor values with increasing sensor array separations; *solid line* $S^+ = 2$; *dashed line* $S^+ = 4$; *dash with dotted line* $S^+ = 8$; *dotted line* $S^+ = 12$ (determined with ideal coefficients); *cross* $S^+ = 8$ (determined with experimental coefficients)

Figure 12 shows the distributions of the turbulent kinetic energy production (above) and dissipation rate (below) for the various array separations. As for the other statistical properties examined above, the array separations of $S^+ = 2$, 4, 8 and 12 are considered for the ideal probe coefficients, as well as $S^+ = 8$ for the real probe coefficients. The differences in the results for the real and ideal coefficients for both production and dissipation rates are small, although somewhat larger near the wall, than for other statistics. The distribution of the production rate is very strongly attenuated due to spatial resolution for $y^+ < 20$ for all sensor separations. The attenuation of the Reynolds shear stress is amplified as the wall is approached because the multiplative mean velocity gradient becomes larger. Some production rate values are only about 1/4 the DNS values in this region. Fortunately, smaller, two-sensor hot-wire probes can be used for production rate measurements. On the other hand, probes with nine or more sensors are needed to measure the full dissipation rate. Fortunately as well, the attenuation of this velocity gradient-based property with increasing sensor separation is not nearly so great as it is for the production rate. Only for an array separation of $S^+ = 12$ is the attenuation very significant for $y^+ < 25$.

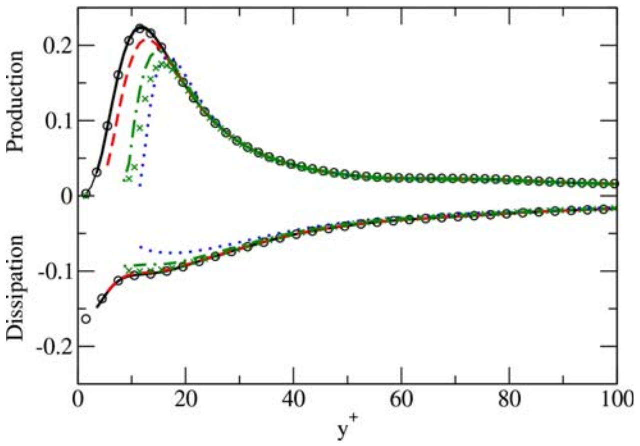

Fig. 12 Resolution effects on the production and dissipation rates with increasing sensor array separations; *solid line* $S^+ = 2$; *dashed line* $S^+ = 4$; *dash with dotted line* $S^+ = 8$; *dotted lines* $S^+ = 12$ (determined with ideal coefficients); *cross* $S^+ = 8$ (determined with experimental coefficients)

8 Conclusions

1. For simulated probe separations of $S^+ = 2$ and 4, the velocity component rms, skewness and flatness values show little change due to spatial resolution compared to the values obtained directly from the DNS except for the skewness values of v in the buffer region and the flatness values of the v and w near the wall.
2. Velocity and vorticity component spectra for the different simulated probe resolutions illustrate the attenuation of the spectral energy with decreasing spatial resolution consistent with the rms results.
3. The velocity component rms values are attenuated less than 10% at $y^+ = 15$ for $S^+ \leq 8$, which is only a slightly better resolution than for a number of laboratory experiments with 9- and 12-sensor probes. Closer to the wall the relative accuracy of the rms values diminishes due to loss of resolution, particularly for the w velocity fluctuations.
4. The attenuation of the vorticity rms values is greatest for the wall normal component, ω_y. For $y^+ = 15$ and $S^+ \leq 8$ it is attenuated not more than 17%. Nearer the wall the attenuation can exceed 20%
5. The skewness factor distributions of the wall normal velocity fluctuations, S(v), display strong dependence on spatial resolution in the buffer layer, explaining the large degree of scatter in this region of data in the literature from experiments and simulations.
6. The skewness factor of the spanwise vorticity component, ω_z, is particularly sensitive to the effects of spatial resolution throughout the channel. The is also true for the flatness factors of ω_y and ω_z.
7. The statistics obtained with ideal and experimental probe coefficients are nearly identical for all of these statistical properties, showing that the experimental probe calibration coefficients account very well for flow blockage by and thermal cross-talk between sensors and the finite lengths of the sensors.
8. The distribution of the turbulent kinetic energy production rate is very strongly attenuated due to spatial resolution for $y^+ < 20$ for all sensor separations. Some production rate values are only about 1/4 the DNS values in this region. Fortunately, smaller, two-sensor hot-wire probes can be used for production rate measurements. The attenuation of the velocity gradient-based dissipation rate with increasing sensor separation is not nearly so large as it is for the production rate. Only for an array separation of $S^+ = 12$ is the attenuation for $y^+ < 25$ very significant. This is fortunate because probes with nine or more sensors are needed to measure this property.
9. The virtual experiment carried out here to examine the resolution effects of varying the array separations of 12-sensor probes was in a low Reynolds number minimal turbulent channel flow. At higher Reynolds numbers where the ratios of the spanwise microscale to the array separations will be smaller, the errors introduced by diminishing spatial resolution will become larger.

Appendix

The a_{ijk} coefficients in Eq. 3 were determined for sensor 1 of array 1 of the ideal probe by expressing the effective cooling velocity as

$$U_e^2 = U^2 \cos^2 \alpha + V^2 \sin^2 \alpha + W^2 - 2UV \sin \alpha \cos \alpha, \qquad (7)$$

where U, V and W are the streamwise, wall normal and spanwise velocity components in the flow coordinate system respectively, and α is the sensor orientation angle between the sensor and the y coordinate direction. The above equation is obtained by setting $k = 0$ and $h = 1$ in Eq. 1 and substituting $U_n = U \cos\alpha - V \sin\alpha$ and $U_b = W$. For $\alpha = 45^\circ$ Eq. 7 becomes

$$U_e^2 = \frac{1}{2} U^2 + \frac{1}{2} V^2 + W^2 - UV. \qquad (8)$$

Comparing Eq. 3 for sensor 1 of array 1 with Eq. 8, it is evident that the values of the coefficients for the ideal probe are $a_{111} = 1/2$, $a_{112} = 1/2$, $a_{113} = 1$, $a_{114} = 1$, $a_{115} = 0$ and $a_{116} = 0$. In like manner, values of the coefficients for the other sensors can be obtained for the ideal probe.

The real a_{ijk} coefficients in Eq. 3 needed for this virtual investigation, together with the b_p coefficients in Eq. 6 that also are needed in a physical experiment, were obtained from the calibration measurements described in

Vukoslavčević and Wallace (1996) carried out in a nominally irrotational calibration jet. The streamwise velocity for the calibration of the 12-sensor probe used in that experiment was varied over a range of 0.6–2 m/s, with pitch and yaw angles ranging from $-20°$ to $+20°$ in steps of 5°. This calibration velocity range covered the mean velocities at positions in the boundary layer where the turbulence measurements were made in that investigation. The extremes of the pitch and yaw range in that calibration corresponded to v and w values in the range of $\pm 0.34u$. For each speed, 45 different U, V and W combinations were induced, giving 45 linear equations. Using a least square fit, these equations were solved for the ten a_{ijk} and b_p (for $p = 1-5$) coefficients for each sensor.

In Vukoslavčević and Wallace (1996) and other papers cited herein, it has been shown that, in this low speed range, the probe response can be accurately described with the combination of (3) and (6) and a properly chosen set of calibration coefficients. For the real probe response presented in the present paper, we took the mean values of the calibration coefficients covering the complete velocity and pitch and yaw angles ranges mentioned above. Better accuracy is obtained if a separate set of calibration coefficients is used for a given value of the local mean streamwise velocity over the whole range of pitch and yaw angles, but this was not necessary for this virtual investigation where the focus is on spatial resolution effects arising from the separation of the virtual sensors. In a real physical experiment, like the one described in Vukoslavčević and Wallace (1996), one can start the calculation with mean values of the calibration coefficients over the whole speed and pitch/yaw range, and then update it with a set that corresponds to the measured value of the local mean streamwise velocity at each measurement position.

References

Andreopoulos Y, Honkan A (1996) Experimental techniques for highly resolved measurements of rotation, strain and dissipation-rate tensors in turbulent flows. Meas Sci Technol 7:1462–1476

Andreopoulos Y, Honkan A (2001) An experimental study of the dissipative and vortical motion in turbulent boundary layers. J Fluid Mech 439:131–163

Antonia RA, Orlandi P, Zhou T (2002) Assessment of a three-component vorticity probe in decaying turbulence. Exp Fluids 33:384–390

Balaras E, Piomelli U, Wallace JM (2001) Self-similar states in turbulent mixing layers. J Fluid Mech 446:1–24

Balint JL (1986) Contribution de l'etude de la structure tourbillionaire d'une couche limite turbulente au moyen d'une sonde a neuf fils chaude measurant le rotationnel. Docteur d'Etat en Sciences Univ. of Lyon, Lyon

Balint JL, Wallace JM, Vukoslavčević P (1991) The velocity and vorticity vector fields of a turbulent boundary layer. Part 2: statistical properties. J Fluid Mech 228:53–86

Cavo A, Lemonis G, Pauidis Th and Papailiou DD (2007) Performance of a 12-sensor vorticity probe in the near field of a rectangular turbulent jet. Exp Fluids 1:17–30

Folz A (1997) An experimental study of the near-surface turbulence in the atmospheric boundary layer. PhD Thesis, University of Maryland, College Park

Galanti B, Gulitsky G, Kholmyansky M, Tsinober A, S Yorish (2004) Adv in turbulence X. In: Andersson HI, Krogstad, P (eds) Proceedings of 10th European turb conf. CIMNE, Barcelona

Honkan A, Andreopoulos Y (1997) Vorticity, strain rate and dissipation characteristics in the near wall region of turbulent boundary layers. J Fluid Mech 350:26–29

Jimenez J, Moin P (1998) The minimal flow unit in near-wall turbulence. J Fluid Mech 225:213–240

Jorgensen F (1971) Directional sensitivity of wire and fibre film probes. DISA Inf 11: 31–37

Kholmyansky M, Tsinober A, Yorish S (2001) Velocity derivatives in the atmospheric turbulent flow at $Re_\lambda = 10^4$. Phys Fluids 13:311–314

Kim J, Moin P, Moser R (1987) Turbulence statistics in fully developed channel flow at low Reynolds number. J Fluid Mech 177:133–166

Kit E, Tsinober A, Balint J-L, Wallace JM, Levich E (1988) An experimental study of helicity related properties of turbulent flow past a grid. Phys Fluids 30:3323–3325

Lemonis G (1995) An experimental study of the vector fields of velocity and vorticity in turbulent flows. PhD Thesis, Swiss Fed Inst of Tech, Zürich

Loucks RB (1998) An experimental investigation of the velocity and vorticity fields in a plane mixing layer. PhD Thesis, University of Maryland, College Park

Marasli B, Nguyen P, Wallace JM (1993) A calibration technique for multiple-sensor hot-wire probes and its application to vorticity measurements in the wake of a circular cylinder. Exp Fluids 15:209–218

Moin P, Spalart PR (1987) Contributions of numerical simulation data bases to the physics, modeling and measurement of turbulence. NASA Tech. Memo 100022

Ong L, Wallace JM (1995) Local isotrophy of the vorticity field in a boundary layer at high Reynolds number. In: Benzi R (ed) Adv. in Turbulence V. Kluwer (Springer), Berlin, pp 392–397

Ong L, Wallace JM (1998) Joint probability density analysis of the structure and dynamics of the vorticity field of a turbulent boundary layer. J Fluid Mech 367:291–328

Park S-Y, Wallace JM (1993) The influence of instantaneous velocity gradients on turbulence properties measured with multi-sensor hot-wire probes. Exp Fluids 16:17–26

Petrović DV, Vukoslavčević PV, Wallace JM (2003) The accuracy of turbulent velocity component measurements by multi-sensor hot-wire probes: a new approach to an old problem. Exp Fluids 34:130–139

Piomelli U, Balaras E, Pascarelli A (2000) Turbulent structures in accelerating boundary layers. J Turbulence 1:Art. No. N1

Pompeo L, Thomann H (1993) Quadruple hot-wire probes in a simulated wall flow. Exp Fluids 14:145–152

Suzuki Y, Kasagi N (1992) Evaluation of hot-wire measurements in wall shear turbulence using a direct numerical simulation database. Exp Therm Fluid Sci 5:69–77

Tagawa M, Tsuji T, Nagano Y (1992) Evaluation of X-probe response to wire separation for wall turbulence measurements. Exp Fluids 12:413–421

Taylor GI (1938) Production and disipation of vorticity in a turbulent fluid. Proc R Soc Lond 164:15–23

Tsinober A, Kit E, Dracos T (1992) Experimental investigation of the field of velocity gradients in turbulent flows. J Fluid Mech 242:169–192

Vukoslavčević P, Wallace JM, Balint J-L (1991) The velocity and vorticity vector fields of a turbulent boundary layer: Part 1 Simultaneous measurement by hot wire anemometry. J Fluid Mech 228:25–52

Vukoslavčević P, Wallace JM (1996) A 12-sensor hot-wire probe to measure the velocity and vorticity vectors in turbulent flow. Meas Sci Technol 7:1451–1461

Vukoslavčević P, Wallace JM (2007) Measurements of the vorticity vector and other velocity gradient tensor based turbulence properties. In: Tropea C, Foss JF (eds) Handbook of experimental fluid mechanics, chap. 5. Springer, Berlin

Wallace JM, Balint J-L, Ong L (1992) An experimental study of helicity density in turbulent flow. Phys Fluids A 4:2013–2026

Wallace JM, Foss JF (1995) The measurement of vorticity in turbulent flows. Ann Rev Fluid Mech 27:469–514

Wyngaard JC, (1969) Spatial resolution of the vorticity meter and other hot-wire arrays. J Sci Instr (J Phys E) Ser 2:983–987

Zhu Y, Antonia RA (1996) Spatial resolution of a 4-X-wire vorticity probe. Meas Sci Technol 7:1492–1497